Journal of Physics: Conference Series **318** (2011) 042006 doi:10.1088/1742-6596/318/4/042006

Wavelet analysis of the slow non-linear dynamics of wave turbulence

Benjamin Miquel & Nicolas Mordant

Laboratoire de Physique Statistique, École Normale Supérieure

E-mail: benjamin.miquel@lps.ens.fr

Abstract. In wave turbulence, the derivation of solutions in the frame of the Weak Turbulence Theory relies on the existence of a double time-scale separation: first, between the period of the waves and caracteristic nonlinear time t_{NL} corresponding to energy exchange among waves; and secondly, between t_{NL} and the characteristic dissipation time t_d. Due to the lack of space and time resolved measurement, this hypothesis have remained unverified so far. We study the turbulence of flexion waves in thin elastic plates. t_d is measured using the decline stage of the turbulence whereas a wavelet analysis is performed to measure the characteristic non-linear time t_{NL}.

1. The Weak Turbulence Theory for thin elastic plates

1.1. The frame of the Weak Turbulence Theory

The Weak Turbulence Theory (WTT) describes the long-time statistical behaviour of a large number of weakly interacting waves. This theory describes numerous systems in various fields: elastic waves in thin plates (1; 2), surface waves in fluids (3), Alfvén waves in astrophysical plasmas (4), ion waves in plasmas (5), etc. Aside its own intrinsec interest, this theory might be considered as an intermediate step toward the comprehension of hydrodynamical turbulence (HT). Indeed, WTT for out-of-equilibrium systems shares a common phenomenology with HT: energy cascading from injection lengths λ_I toward dissipation lengths λ_D builds a continuous Kolmogorov-Zakharov spectrum $E^{KZ}_{\mathbf{k}}$ (6). In contrast with hydrodynamical turbulence, many analytical predictions – including the analytical derivation of the spectrum – are made possible by the WTT strong hypothesis: (i) the size of the system is asymptotically large and (ii) the interactions between waves are weak. Mathematically, these hypotheses lead to a multiscale treatment of the equation of the motion. On a more physical ground, the motion is composed of wavetrains exchanging energy at a slow rate compared to the period of the waves.

1.2. Theoretical predictions for thin plates

The WTT formalism was applied to the specific case of flexion waves propagating on an elastic plate by Düring (7). The deformation field of the plate ζ obeys a Föppl-Von Karman equation (7; 8) featuring a linear term due to bending and a nonlinear correction due to stretching. The linear term yields a quadratic dispersion relation for the linear waves $\omega_{\mathbf{k}} = ck^2$ (with $k = |\mathbf{k}|$). The analytical derivation of the spectrum necessitates the introduction of the canonical variables $a_{\mathbf{k}}$. These variables diagonalize the linear part of the hamiltonian. One then

defines the wave occupation number $n_{\mathbf{k}} =< a_{\mathbf{k}} a^*_{\mathbf{k}} >_{\text{stat}}$ ($< . >_{\text{stat}}$ and * stands for statistical average and complex conjugaison, respectively). The occupation number is found to obey a kinetic equation:

$$\frac{\partial n_{\mathbf{k}}}{\partial t} = F_{\mathbf{k}} + \mathcal{C}oll\left(\{n_{\mathbf{k}}\}\right) - \gamma_{\mathbf{k}} n_{\mathbf{k}} \tag{1}$$

Forcing $F_{\mathbf{k}}$ and dissipation $\gamma_{\mathbf{k}} n_{\mathbf{k}}$ are localized in long and short wave-lengths, respectively. The conservative collision integral $\mathcal{C}oll\left(\{n_{\mathbf{k}}\}\right)$ transfers energy between resonant wavetrains. In WTT, forcing and dissipation are well separated in Fourier space and circumscribe the transparency window: for wavelengths λ such that $\lambda_I \gg \lambda \gg \lambda_D$, $\mathcal{C}oll\left(\{n_{\mathbf{k}}\}\right)$ is the leading order term of the RHS of equation (1) so that energy is transferred conservatively. The Kolmogorov-Zakharov (KZ) spectrum is a stationnary out of equilibirum solution that cancels the collision term $\mathcal{C}oll\left(\{n_{\mathbf{k}}\}\right)$. The predicted wave occupation spectrum $n_{\mathbf{k}}$ and predicted power spectrum of velocity $E_{\mathbf{k}} \propto k^2 n_{\mathbf{k}}$ reads:

$$n^{KZ}_{\mathbf{k}} = C P^{1/3} k^{-2} \ln^{1/3}\left(k_c/k\right) \quad , \quad E^{KZ}_{\mathbf{k}} = C' P^{1/3} \ln^{1/3}\left(k_c/k\right) \quad , \quad E^{KZ}_{\omega} = C'' P^{1/3} \ln^{1/3}\left(\omega_c/\omega\right) \tag{2}$$

In the stationnary regime, P is the averaged injected and dissipated power, C is a constant depending on the properties of the plate and k_c is a cutoff wave-number. In the mean time, the non-linearities are responsible for a small departure $\delta\omega$ from the quadratic dispersion relation of the linear problem. This correction is predicted to share a common power law in P with the KZ spectrum.

1.3. Setup and experimental (dis)agreements in the stationary regime

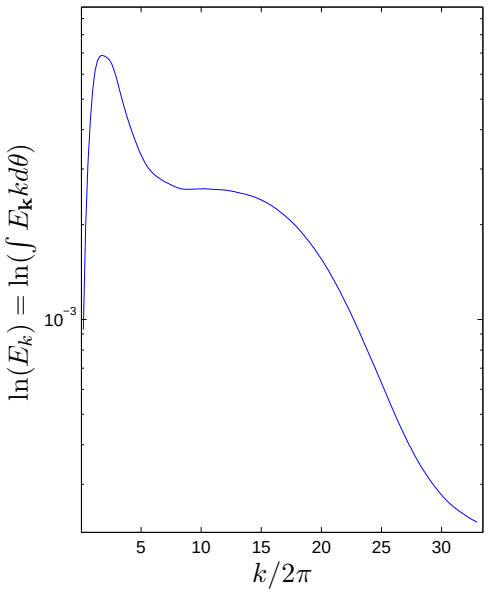

Figure 1. Plain blue line: Integrated over angles spectrum. Note (as k increases): the noticeable forcing at small wavevectors; the flat plateau corresponding to a power-law spectrum; the logarithmic cut-off

Our system consists of a thin flat stainless plate (0.4 mm $\times$ 1 m $\times$ 2 m) hanging with no stress but its own weight. An electromagnetic shaker acts as a point source of vibration at the frequency $\nu_f = 30$ Hz. We measure the motion of the plate using an optical profilometry method developped by Cobelli *et al.* (9) performed with a high speed camera. From the measured normal

deformation field $\zeta(\mathbf{r},t)$ we compute the velocity field $v(\mathbf{r},t) = \partial_t \zeta$ and its space-time Fourier transform $\tilde{v}_{\mathbf{k},\omega}$. A statistical average on realisations yields the space-time power spectrum :

$$E_{\mathbf{k},\omega} = < \tilde{v}_{\mathbf{k},\omega} \tilde{v}^*_{\mathbf{k},\omega} >_{\text{stat}} \tag{3}$$

As predicted, the energy is found to be localized in the vicinity of the surface given by the dispersion relation $\omega_{\mathbf{k}} = ck^2$ in the Fourier space. We measure $c = 0.641 \pm 0.001$ $s^{-1}.m^{-2}$ for our stainless steel plate. This result constitute a strong clue in favor of a motion composed of waves. When integrated over wave vector, the space-time spectrum leads to the experimental frequency spectrum $E^{exp}_{\omega} \propto \omega^{-0.6} P^{0.7}$ (1). This spectrum does not exhibit the theoretical exponent (eq (2)) for frequency ω nor for injected power P. However the frequency spectrum and the correction to the linear dispersion relation $\delta\omega$ share a common power law, as predicted by WTT.

1.4. Decline stage: dissipative time

The plate is first shaken until the stationary regime is reached. The forcing is then stopped and the deformation of the plate is recorded and analyzed in the same fashion than the stationary case. The cut-off wavenumber k_c decreases with the energy contained in the *cascade*. For a wavevector initially located in the *cascade* ($k_0 < k_c^{stat}$), energy transfer to higher wave number modes are responsible for the evolution of the energy of the mode k_0 at early dates after the stop of the forcing. As $k_c(t)$ crosses k_0, the mode k_0 enter the dissipative part of the spectrum where the energy decay is no longer attributed to transport but dominantly to dissipation. These two steps are exhibited on figure 2. The dissipative rates of every modes $\gamma_{\mathbf{k}}$ are measured by fitting the dissipative part of the spectrum with an exponential decay $\propto \exp(-\gamma_{\mathbf{k}} t)$ (dashed lines on figure 2). The dissipative time t_d is clearly separated from the period of the wave $T = 2\pi/\left(ck^2\right)$ (figure 3): $t_d = 25T$ at the forcing scale up to $t_d = 100T$ at $k/2\pi = 25m^{-1}$. This separation opens the possibility for a non linear time to stand between t_d and T.

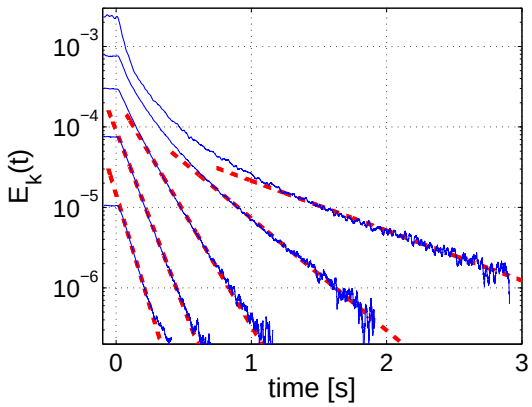

Figure 2. Integrated over angle spectrum $E_k(t) = \int E_{\mathbf{k}} k \mathrm{d}\theta$ as a function of time plotted for 4 different wavevectors (solid blue line) on a semilog scale. Curves are shifted vertically for lisibility. Red thick dashed line are exponential fits $\exp(-\gamma_{\mathbf{k}} t)$ of the dissipative part of each spectrum.

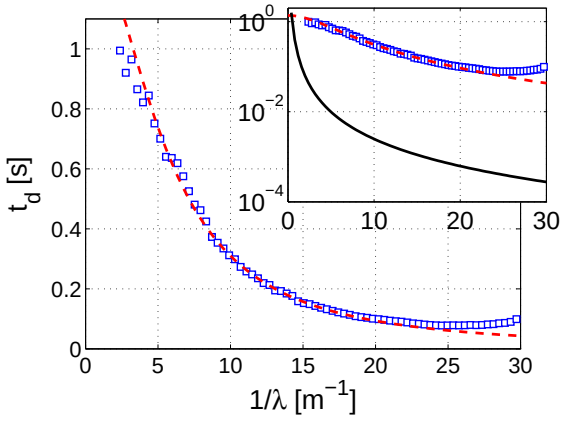

Figure 3. Blue square □: Measured dissipative time $t_d(\mathbf{k}) = 1/\gamma_{\mathbf{k}}$ plotted versus k. Red dashed line: Lorentzian fit $t_d = \left(0.73 + 0.025(k/2\pi)^2\right)^{-1}$ (s). Insert: t_d (□), lorentzian fit (red dashed line) and period of the waves T (solid black line) versus k on a semilog scale.

2. Non-linear dynamics

2.1. One definition of the non-linear time t_{NL}

Since the motion is predicted to be a superposition of wavetrains, we carry out a method measuring the dynamics of one wave packet embedded in a turbulent ensemble of waves. The spatial Fourier transform of the velocity $\tilde{V}_{\mathbf{k}}(t)$ is thus expected to oscillate rapidly at the pulsation $\omega_{\mathbf{k}}$ with a slow modulation $\tilde{v}_{\mathbf{k}}$:

$$\tilde{V}_{\mathbf{k}}(t) = \tilde{v}_{\mathbf{k}}(t) \exp\left(\mathrm{i}\omega_{\mathbf{k}} t\right) \tag{4}$$

The slow variation of the envelop of V are described by the autocorrelations of $\tilde{v}_{\mathbf{k}}$:

$$\mathcal{G}_{\mathbf{k}}(t) = < \tilde{v}_{\mathbf{k}}(T+t)\tilde{v}^*_{\mathbf{k}}(T) >_{\mathrm{stat}} \tag{5}$$

We define the non-linear time as $t_{NL}(\mathbf{k})$ using $\mathcal{G}_{\mathbf{k}}$:

$$t_{NL}(\mathbf{k}) = \int_0^\infty \frac{\mathcal{G}_{\mathbf{k}}(t)}{\mathcal{G}_{\mathbf{k}}(0)} \mathrm{dt} \tag{6}$$

Although t_{NL} is defined with $\tilde{v}$, a direct experimental estimation is difficult. First it would require to measure the deformation over the whole system, and second computing $\tilde{v}$ from the measured $\tilde{V}$ by simply multiplying by a phase $\mathrm{e}^{-\mathrm{i}\omega_{\mathbf{k}}t}$ would require a very precise knowledge of $\omega_{\mathbf{k}}$. The next section introduces a method based on wavelets analysis in order to compute t_{NL}.

2.2. Decomposition of the turbulent motion on the wavelet family

We use 2D Gabor wavelets that are characterized by the position $\mathbf{R}$, the wave vector $\mathbf{k}_0$ and a Gaussian envelop of width σ (fig. 4):

$$w_{\mathbf{k}_0,\mathbf{R},\sigma}(\mathbf{r}) = (\sigma\sqrt{\pi})^{-1} \exp(\mathrm{i}\mathbf{k}_0 \cdot \mathbf{r}) \exp\left(-\frac{(\mathbf{r}-\mathbf{R})^2}{2\sigma^2}\right) \tag{7}$$

We emphasize that although our study is performed using Gaussian wavelets for tractability sake, the method is robust: the results are independent of the envelop of the wavelet $w_{\mathbf{k}_0,\mathbf{R},\sigma}(\mathbf{r}) = \mathcal{E}_{\mathbf{R},\sigma} \exp\left(\mathrm{i}\mathbf{k}_0\mathbf{r}\right)$ where the envelop $\mathcal{E}$ may be any usual windowing function (hanning, tukey, etc.).

Let $a_{\mathbf{k}_0,\mathbf{R},\sigma}(t)$ be the wavelet component of $V(\mathbf{r},t)$ (along the wavelet $w_{\mathbf{k}_0,\mathbf{R},\sigma}(\mathbf{r})$):

$$a_{\mathbf{k}_0,\mathbf{R},\sigma}(t) = \int V(\mathbf{r},t) w^*_{\mathbf{k}_0,\mathbf{R},\sigma}(\mathbf{r}) d\mathbf{r} = \int \tilde{V}(\mathbf{k},t) \tilde{w}^*_{\mathbf{k}_0,\mathbf{R},\sigma}(\mathbf{k}) d\mathbf{k} \tag{8}$$

We define the autocorrelation $\mathcal{A}_{\mathbf{k}_0,\mathbf{R},\mathbf{R}'}$ and the crosscorrelation $\mathcal{C}_{\mathbf{k}_0,\mathbf{R},\mathbf{R}'}$ of the wavelets coefficients ($< . >_T$ denote the average over the time T):

$$\mathcal{A}_{\mathbf{k}_0,\mathbf{R},\mathbf{R}'}(t) = \left\langle a^*_{\mathbf{k}_0,\mathbf{R}}(T) a_{\mathbf{k}_0,\mathbf{R}'}(T+t) \right\rangle_T \tag{9}$$

$$\mathcal{C}_{\mathbf{k}_0,\mathbf{R},\mathbf{R}'}(t) = \left\langle a^*_{\mathbf{k}_0,\mathbf{R}}(T) a_{-\mathbf{k}_0,\mathbf{R}'}(T+t) \right\rangle_T \tag{10}$$

The correlation $\mathcal{A}$ measures the temporal coherence of the wavepaquet $w_{\mathbf{k},\mathbf{R}}$ embedded in the turbulent field at time T and the wavepaquet $w_{\mathbf{k},\mathbf{R}}$ at time $T+t$. $\mathcal{C}$ measures the same thing but beween two packets propagating in opposite directions.

The case of a wide ($\sigma k_0 >> 1$) Gaussian wavepacket is analytically tractable and yields:

$$\mathcal{A}_{\mathbf{k}_0,\mathbf{R},\mathbf{R}'} = \mathcal{G}_{\mathbf{k_0}}(t) \frac{1}{\sqrt{1+\frac{c^2t^2}{\sigma^2}}} e^{-\frac{(\mathbf{R}'-(\mathbf{R}+\mathbf{v}_g t))^2}{4\sigma^2\sqrt{1+\frac{c^2t^2}{\sigma^2}}}} e^{-\mathrm{i}\omega_{\mathbf{k}_0}t} e^{\mathrm{i}\Phi(t)} \tag{11}$$

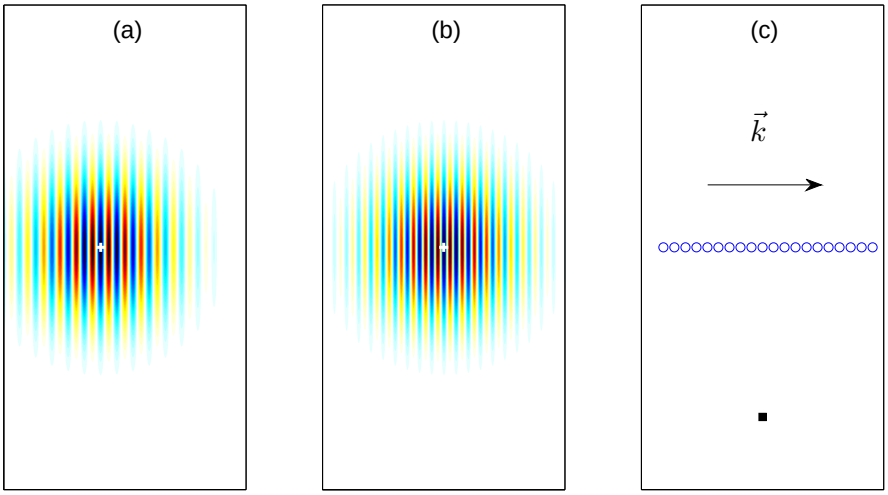

Figure 4. Figures (a–b): examples of Gaussian wave packets in a 2 m × 1 m plate, with $\sigma = 20$ cm. The position $\mathbf{R}$ is marked by a white cross (+). (a) $k/2\pi = 15$ m^{-1}. (b) $k/2\pi = 20$ m^{-1}. (c) Layout of the plate. ■position of the shaker; ○ centers of the wavelets $\mathbf{R}_i$; the black arrow is the direction of the wavevectors $\mathbf{k}$

The correlation function of the slow modulation $\mathcal{G}_{\mathbf{k}_0}(t)$ illustrates the energy transfer between the wave packet we are tracking and the surrounding turbulent bath. The other coefficients account for the dispersion of the Gaussian wavepacket: the wave packet initially located around $\mathbf{R}$ has broadened and propagated during the time t at the position $\mathbf{R} + \mathbf{v}_g t$. The detailed expression of the phase factor $\Phi(t)$ is not relevant in the following analysis. The derivation of equation (11) will be detailed in a forthcoming article. Using this analytical expression in the case of a Gaussian wavepacket, we compute the compensated autocorrelation coefficients $\mathcal{A}'$ to correct the decay due to the dispersion:

$$\mathcal{A}'_{\mathbf{k},\mathbf{R},\mathbf{R}'}(t) = \sqrt{1+\frac{c^2t^2}{\sigma^2}}\mathcal{A}_{\mathbf{k},\mathbf{R},\mathbf{R}'} \tag{12}$$

$$|\mathcal{A}'_{\mathbf{k},\mathbf{R},\mathbf{R}'}(t)| = |\mathcal{G}_{\mathbf{k}}(t)|\mathrm{e}^{-\frac{(\mathbf{R}'-(\mathbf{R}+\mathbf{v}_g t))^2}{4\sigma^2\sqrt{1+\frac{c^2t^2}{\sigma^2}}}} \tag{13}$$

2.3. Measured wavelets coefficients correlations

For sake of simplicity, we study wave packets propagating along the direction given by the short side of our plate. The wavelet coefficients are computed for several positions $\mathbf{R}_i$ (see figure 4), and different wavenumbers from forcing to dissipation. The width of the wavelets is $\sigma = 15$ cm. Thereby the wavelet is well located in Fourier space but still fits in the plate. Some corrected correlation coefficients are plotted in figure 5. Figure 5(a) displays the autocorrelations at the

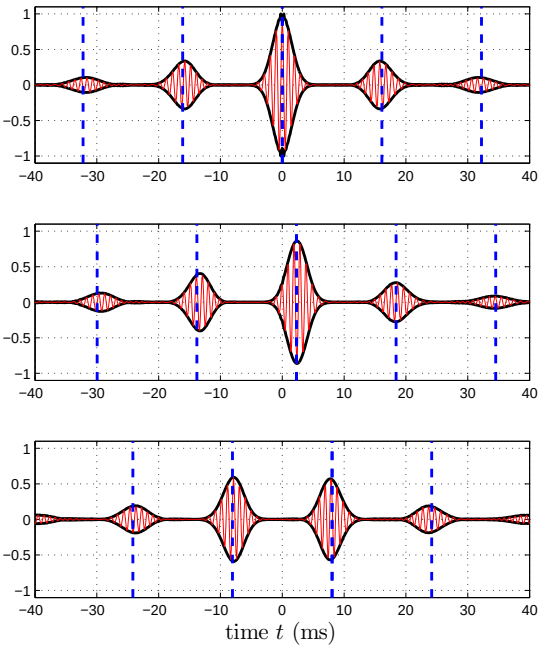

Figure 5. Real part (red thin line) and modulus (black thick line) of some wavelets coefficients correlations fonctions $\mathcal{A}_{\mathbf{k},\mathbf{R},\mathbf{R}'}(t)$ versus time. $|\mathbf{k}/(2\pi)| = 16$ m^{-1}, $v_g = 2ck = 129$ m.s^{-1}, $L/v_g = 7.8$ ms. Note the $2L/v_g$-periodic maxima due to reflexions:
(a) $\mathbf{R} = \mathbf{R}'$;
(b) $\mathbf{R}' = \mathbf{R} + \Delta\mathbf{R}$ with $\Delta R = 30$ cm. The main maximum is delayed from 0 by $\Delta t = \Delta R/v_g = 2.3$ ms;
(c) cross-correlations $\mathcal{C}$ for $\mathbf{R} = \mathbf{R}'$. Main maximum for $t = L/v_g$.

same position ($\mathbf{R} = \mathbf{R}'$). The envelop of the correlation decays quickly to zero as the wave packet is moving at the group velocity away from its initial position (the width of the envelop around $t = 0$ is related to the width of the envelop of the wavelet). Other peaks of the envelop of the correlations are seen that are due to the rebounds of the wave packet at the border of the plate: one rebound on each side is required for the wave packet to come back to its initial position with the same $\mathbf{k}$ (as $\mathbf{k}$ is turned into $-\mathbf{k}$ at each rebound) so that a maximum of correlation is observed every $2L/v_g$. The amplitude of the maxima decays with the number of rebound pairs due to the decoherence of the wave packet related to energy exchanges with the other waves contained in the turbulent field. When looking at autocorrelation between different positions, according to equation (13), compensated autocorrelations coefficients exhibit a maximum for $t_{\max} = |\mathbf{R}' - \mathbf{R}|/v_g$:

$$\left|\mathcal{A}'_{\mathbf{k},\mathbf{R},\mathbf{R}'}\left(\frac{\mathbf{R}'-\mathbf{R}}{v_g}\right)\right| = \left|\mathcal{G}_{\mathbf{k}}\left(\frac{\mathbf{R}'-\mathbf{R}}{v_g}\right)\right| \tag{14}$$

as can be seen in figure 5(b). For the cross correlation $\mathcal{C}$ at the same position (fig. 5(c)), similar features are observed: the cross-correlation is zero at $t = 0$ and the first maximum occurs after one rebound on a side of the plate (i.e. at $t = L/v_g$ if $\mathbf{R}$ is the center of the plate) and then a maximum every $2L/v_g$. As a consequence, seeking the maxima of $\mathcal{A}$ and $\mathcal{C}$ for different position pairs is a way of measuring $|\mathcal{G}_{\mathbf{k}}|$ at different times.

2.4. Discussion about t_{NL}

We gather on figures 6 the envelop of the autocorrelation and cross correlation coefficients for a given $\mathbf{k}$ but different relative positions. The positions of the maxima are measured and fitted with an exponential decay (insert of figure 6) which characteristic time provides the non linear time t_{NL}. We plot $t_{NL}(\mathbf{k})$ as a function of $\mathbf{k}$ at a given forcing intensity P on figure 7. For small k (long wavelength) our analysis is not valid as the condition $\sigma k >> 1$ is no longer fulfilled.

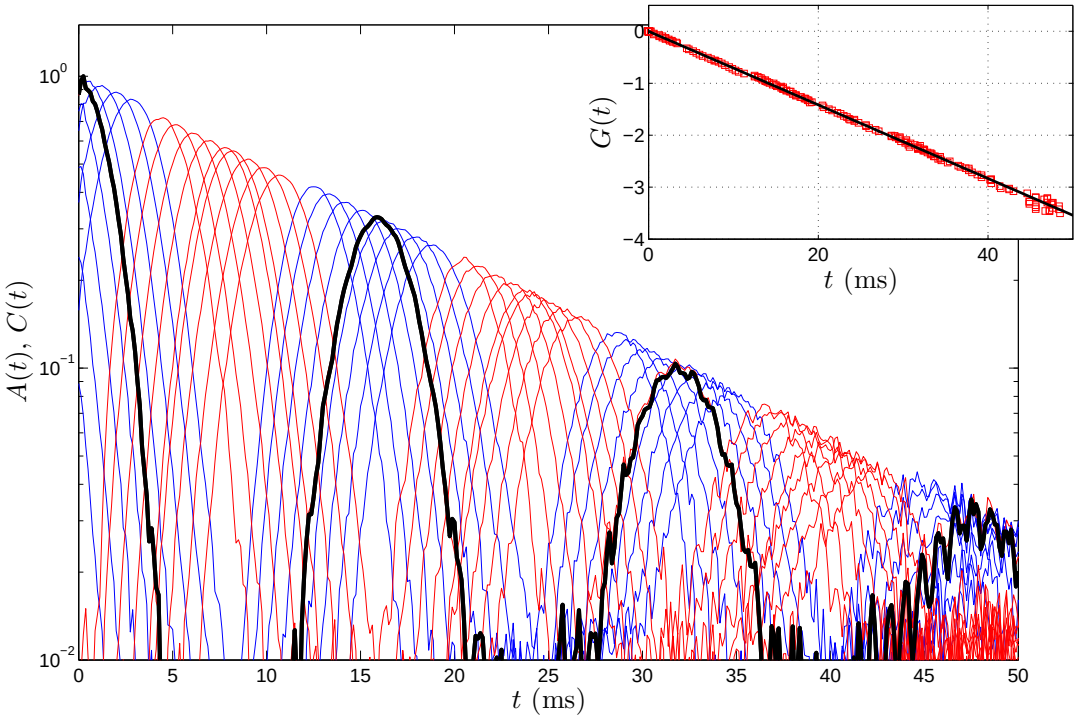

Figure 6. Correlations as a function of time (in ms) for $k/(2\pi) = 15$ m^{-1}. Black thick line: Autocorrelation at the same position $\mathcal{A}_{\mathbf{k},\mathbf{R},\mathbf{R}}$; blue lines: autocorrelations $\mathcal{A}_{\mathbf{k},\mathbf{R},\mathbf{R}'}$; red lines: crosscorrelations $\mathcal{C}_{\mathbf{k},\mathbf{R},\mathbf{R}'}$. Insert: measured maxima (□) and fit $\mathcal{G}(t) = \exp -t/t_{NL}$ with $t_{NL} = 14.1$ ms (black thick line)

Beyond $k/2\pi = 29$ m^{-1}, the signal over noise ratio for correlations is very poor as the signal drops very quickly to zero. Hence these points are absent from figure 7. From the decreasing spectrum displayed in figure 1, one expect the coherence of wavepackets to subsist on longer times (as compared to the period of the wave) as k increases. Our datas verify this prediction since t_{NL} is slightly increasing with k whereas the period of the wave decays as $1/k^2$.

The double scale separation validity is investigated by computing the ratios that compare dissipation and non-linearities $Q_d = t_d/t_{NL}$ or non-linearities and wave period $Q_\omega = t_{NL}\omega$ (displayed in figure 7). The separation between dissipative and non-linear effects is well verified, even in the quite advanced dissipative part of the spectrum: $Q_2 > 5$ for $k = 20$ m^{-1}. This scale separation validates the hypothesis of the existence of a transparency window.

2.5. Frozen turbulence

The size of our system is finite (width L) so that the modes are discrete in Fourier space, and two contiguous modes are separated in $k-$space by $\delta k = \pi/L$. In the regular turbulent regime, the effect of non linearity results in a broadening of each mode that overcomes the distance between modes: $\delta k_{NL} > \pi/L$. Using the dispersion relation, this inequality yields:

$$t_{NL} < T_{\text{froz.}} \quad \text{with} \quad T_{\text{froz.}} = L/(2\pi ck) \tag{15}$$

The regular turbulent regime is characterized by a continuous ensemble of accessible wave vectors due to the broadening of the discrete modes. If the inequality is verified, a finite size system

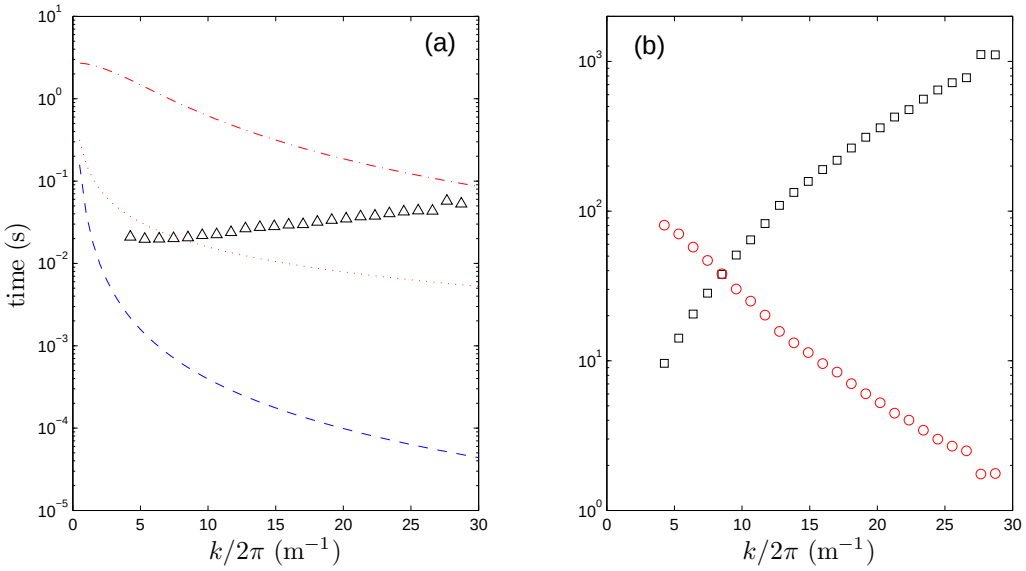

Figure 7. (a) Triangles (△): Measured non-linear time t_{NL} for a given amplitude of forcing versus $\mathbf{k}/2\pi$. Dashed line: period of the waves. Dotted line: $T_{\text{froz.}} = L/(2\pi ck)$. Dashed-dotted line: dissipative time t_d. (b) Squares (□): $t_{NL}\omega$; Circles (○): ratio t_d/t_{NL}.

resembles an infinite system so that hypothesis (i) is met although being not rigorously verified. On the contrary, if $t_{NL} \gg T_{\text{froz.}}$ the modes are clearly separated and the system behaves rather like a finite dimensional non linear system. The resonance conditions may be difficult to fulfill for discrete modes and the energy transfer is more difficult or even frozen depending on the cases (see reference (11) for frozen turbulence). The ratio $t_{NL}/T_{froz.}$ increases with k at a given injected power P so that frozen turbulence appears for large k. Although the energy flux in Fourier space may be strongly different to that of the continuous case and be zero in some cases, the phase of each mode is still randomized by the chaotic exchange of energy among the modes. In an intermediate regime $t_{NL} \sim T_{froz.}$ the cascade is altered by the finite size effects but can still transfer energy among scales. This situation seems to correspond to our case and may explain the disagreement between the observed scaling of the spectra and the theoretical one.

3. Conclusion

We measured the dissipative time and the non-linear time as a function of k. The double time-scale separation stated by the WTT is well verified. Nevertheless the experimental spectrum of the wave is in disagreement with the theoretical prediction. This is explained by the occurrence of finite size effects that alter the cascade.

Acknowledgments

This work was funded by the french Agence Nationale de la Recherche under grant TURBONDE BLAN07-3-197846.

References

[1] Mordant, N.: Fourier analysis of wave turbulence in a thin elastic plate, *Eur. Phys. J. B* **76**: 537-545, 2010

[2] Boudaoud, A., Cadot, O., Odille, B., Touzé, C.: Observation of wave turbulence in vibrating plates, *Phys. Rev. Lett.* **100**: 234504, 2008

[3] Falcon, E., Laroche, C. and Fauve, S.: Wave turbulence on a fluid surface, *Phys. Rev. Lett.* **98**: 094503, 2007

[4] Sagdeev, R. Z., *Rev. Mod. Phys.* **51**: 1, 1979

[5] Mizuno, K. and DeGroot, J. S. *Phys. Fluids* **26**: 608, 1983

[6] Zakharov, V.E., L'vov, V.S., Falkovich, G.: *Kolmogorov Spectra of Turbulence I.* Springer, Berlin, 1992.

[7] Düring, G., Josserand, C., Rica, S.: Weak turbulence for a vibrating plate: can one hear a Kolmogorov spectrum ? *Phys. Rev. Lett.* **97**: 025503, 2007.

[8] Landau ,L. and Lifchitz, E.: *Theory of elasticity*, MIR, Moscou, 1967

[9] Cobelli, P., Petitjeans, P., Maurel, A., Pagneux, V.: Experimental and theoretical inspection of the phase-to-height relation in Fourier transform profilometry, *Applied Optics* **48**: 380, 2009

[10] Miquel, B., Mordant, N.: Non stationary wave turbulence in an elastic plate, *Phys. Rev. Lett., in press*

[11] Kartashova, E., *EuroPhys. Lett.* **87**: 44001, 2009